Active sites for HDS on (Pt,Co)MoS2 catalysts are also active for HER reaction: A proof of concept

L.A. Zavala-Sanchez, X. Portier, F. Maugé, Laetitia Dubau, L. Oliviero

Active sites for HDS on (Pt,Co)MoS_2 catalysts are also active for HER reaction: a proof of concept

L. A. Zavala-Sanchez[1], X. Portier[2], F. Maugé[1], L. Dubau[3], L. Oliviero[1*]*

[1] Laboratoire Catalyse et Spectrochimie, Normandie Université, ENSICAEN, UNICAEN, 6, bd du Maréchal Juin, 14050 Caen, France.

[2]Centre de recherche sur les Ions, les Matériaux et la Photonique, CEA, UMR CNRS 6252, Normandie Université, ENSICAEN, UNICAEN, CNRS, 6, bd du Maréchal Juin, 14050 Caen, France.

[3]Univ. Grenoble Alpes, CNRS, Grenoble INP, Univ. Savoie Mont Blanc, LEPMI, 38000 Grenoble, France

*Corresponding Authors:

Laetitia Oliviero (HDS, characterization) orcid.org/0000-0002- 7931-439X

E-mail: laetitia.oliviero@ensicaen.fr

Laetitia Dubau (HER) orcid.org/0000-0001-9520-1435

Email: laetitia.dubau@grenoble-inp.fr

ABSTRACT

Molybdenum sulfide catalysts are considered of interest in the aim to find alternative to the Pt/C reference catalyst for electrocatalyzed Hydrogen Evolution Reaction (HER). Known since decades as hydrotreatment catalysts, their characterization has been widely detailed in order to draw structure-activity relationship and to optimize their design and preparation. In this study, we aim to draw a parallel between the catalytic activity in a model hydrodesulfuration (HDS) reaction and the one in electrocatalysis for HER reaction in order to verify that the optimization of the edge sites properties for HDS could also be beneficial for HER reaction.

1. INTRODUCTION

Finding a replacement for conventional fossils fuels with clean and affordable energy is a critical concern of modern world. An essential factor for the development of transport technologies is the need for green and sustainable energy sources with a tolerable environmental impact for the growing world population.[1] Hydrogen is an ideal vector of high energy density in mass basis,

since it can convert chemical energy into clean electrical energy in fuel cell devices, where the by-product is only water.[2] Besides being a sustainable energy carrier, it has the potential of substituting fossil fuels, and by this way decreasing carbon dioxide (CO_2) emissions.[3] In this regard, electrochemical water splitting ($H_2O \rightarrow H_2 + ½\ O_2$) is a promising and attractive way to store sustainable, intermittent energy resources in the form of hydrogen.[4] Electrocatalytic water splitting could efficiently produce hydrogen directly from water, and the electrical energy that drives the water splitting could be harvested from renewable solar power or wind power.[5] In a water electrolyzer, the hydrogen evolution reaction (HER) takes place at the cathode and is globally expressed as follows:

$$2H^+ + 2e^- \rightarrow H_2$$

The hydrogen evolution reaction is thought to involve three possible reaction steps:

$$\text{Volmer step: } H^+ + e^- \rightarrow H_{ads} \qquad \text{(eq. 1)}$$

$$\text{Heyrovsky step: } H^+ + H_{ads} \rightarrow H_2 \qquad \text{(eq. 2)}$$

$$\text{Tafel step: } 2\ H_{ads} \rightarrow H_2 \qquad \text{(eq. 3)}$$

The relationship between the overpotential and current density is shown in Equation 4 (Tafel's equation), where η is the overpotential, j is the current density, a is the intercept associated to the exchange current density j_0, and b is the Tafel slope.

$$\eta = a + b \times \text{Log}\,|j| \qquad \text{(eq. 4)}$$

Generally, the Tafel slope is used to reveal the inherent reaction processes of HER, because it is determined by the rate determining step ((RDS) of HER. By comparing the empiric obtained slope for a certain catalyst with the theoretical values, it is possible to predict the main mechanism (Volmer-Heyrovsky or Volmer-Tafel) and determine the RDS.

The great interest of the scientific community in electrocatalysis for the hydrogen evolution reaction (HER) is reflected in the large number of publications on the production of H_2. Nevertheless, one of the main challenges is the development of a sustainable and efficient catalyst, which can also maintain adequate stability. Up to now, Pt nanoparticles (NPs) with a diameter $2 < d < 5$ nm supported on high-surface-area carbon are the benchmark for HER catalytic efficiency in acidic conditions.[6] An outstanding catalyst in electrocatalysis must meet

several standards, including low overpotential, low Tafel slope, and high exchange current density. However, the high cost of Pt and the necessary high load for effectiveness, in addition to its scarcity, makes it a non-scalable material for large-amount hydrogen generation. Up to now, it has not been reported a catalyst that has shown better HER performance than Pt.[7]

Molybdenum sulfide nanoparticles, has received much attention and has become a promising alternative for its low cost, earth abundance and HER catalytic activity and stability in acidic conditions.[8,9] Overall, MoS_2 contains four different crystal structures, which are 1H, 1T, 2H, and 3R. MoS_2 generally has 2H (hexagonal) structure with semiconductive properties, while 1T (tetragonal) phase exhibits a metallic character. [10] Due to the semiconductive character of MoS_2 based materials, the coupling of MoS_2 with a highly conductive support is essential to improve its catalytic activity. For this purpose, carbon materials, such as porous high surface area carbon black, are considered as a great catalytic support in electrocatalysis due to their high conductivity and stability. Therefore, supporting transition metal disulfides (TMD) on carbon materials could be a feasible and promising way to improve their performance.[11]

The two-dimensional (2D) molybdenum sulfide (MoS_2) nanostructure (slab) has proven to be one of the most important materials with diverse applications in hydrotreatment.[12–15] While supported MoS_2 promoted by Co and/or Ni has been used for years in the hydrodesulfurization (HDS) process to remove sulfur from crude oil feedstock, the use of promoted MoS_2 in the hydrogen evolution reaction (HER) brings renewed interests in these catalyts.

Hinneman et al. reported that the low hydrogen adsorption free energy ($\Delta G°_H \sim 0.0$) is a good descriptor of materials that can catalyze hydrogen evolution and applies to a wide range of systems.[16] HDS and HER involve similar mechanism steps where there is a key intermediate H_{ads}.[5] In case of HDS, the hydrogen serves multiple roles: generation of anion vacancy by removal of sulfide, hydrogenation, and hydrogenolysis. In HER, the S atoms on the exposed edges of MoS_2 based catalysts could strongly bond with the H^+ ions in solution, at the initial step of the reduction process, allowing the effective reduction of H^+ ions to H_2.[11] Therefore, it is reasonable to consider that an HDS catalyst will be performant too as a HER electrocatalyst.

Theoretical and experimental studies have suggested that the HER activity mainly arises from the sites located along the edges of the MoS_2 slab,[4] while the basal surface is mainly catalytically inert. However, it has been documented that the basal plane can be activated by insertion of

transition metals atoms (doping) [17,18]. Despite the good results obtained when doping in the basal plane, the integrated atoms turn out to be scarce and their insertion appears to be less controlled. While the integration of atoms at the edges is more conducive as well as better documented. Recently, we found that conventional 2H MoS_2 sequentially doped with cobalt (Co) then 1 wt. % of Pt showed improved HER activity[19]. This result is attributed to the favorable modification of H bonding energy of MoS_2 edge active sites (since the promoting atoms are mostly located at the edges).

Since bulk MoS_2 presents low catalytic activity for HER because of low edge site concentration, , MoS_2 should be in nanostructured supported form. to increase the exposed edge/basal atomic ratio. Moreover, one proven way to increase further this ratio by decreasing the MoS_2 particle size is adding a chelating agent such as citric acid (CA) [20]. Also, the addition of CA can help to moderate the particle agglomeration and facilitate discrete growth of active sites on supports.[21] Our group has explored intensively the effect of citric acid as a chelating agent.[20,22–25] The use of citric acid (CA) has been well-documented as an effective method of preparing highly HDS active CoMo catalyst.[22,24] favoring the edge Co promotion.

In this work, we aim to demonstrate that the activity ranking of MoS_2 catalysts is indeed similar between HER and HDS reactions and in particular that citric acid addition during impregnation has also a positive effect on the HER performance. Consequently, we prepared several series of promoted and non-promoted catalysts and tested them in HDS model reaction and HER.

2. EXPERIMENTAL

2.1. Preparation of the catalysts with and without citric acid addition

Three series of mono- bi- and trimetallic (MoS_2/C, Co-MoS_2/C and $Pt_{1\%}$-$CoMoS_2$/C) catalysts with different amounts of citric acid (CA) were prepared by an incipient wetness impregnation method, following a previously reported method.[20,23,24,26] As support, carbon black (Vulcan XC 72 Cabot Corp., specific surface area of 223 $m^2.g^{-1}$ and pore volume of 0.41 $ml.g^{-1}$) was used, as-received. The aqueous impregnation solutions were prepared with a defined amount of ammonium heptamolybdate tetrahydrate ($(NH_4)_6Mo_7O_{24}\cdot 4H_2O$, Merck). For the Co-promoted MoS_2 sample, (Co $(NO_3)_2\cdot_6H_2O$, Alfa Aesar) was used with an atomic ratio equal to Co/Co+Mo=

0.3. For the $Pt_{1\%}$-$CoMoS_2$/C sample, tetraammine platinum (II) nitrate $(NH_4)_2Pt(NO_3)_2$, Sigma-Aldrich) was used. In the three series, citric acid ($C_6H_8O_7 \cdot H_2O$, Prolabo) amount was varied in order to obtain CA/M = 0, 1 2 or 3 (M=Mo+Co+ Pt). The catalysts were named according to their mono- bi- and trimetallic nature and according to the value of CA/M=x molar ratio given as CA= x.

After impregnation, the catalysts were dried for 12 h at 393 K to preserve the species formed in presence of citric acid up to the sulfidation stage (no calcination step). All catalysts samples were prepared with a constant amount of Mo, Co, and Pt corresponding to 15 wt % Mo, 3 wt % Co and wt 1% Pt. Later the oxide catalysts were sulfided in a glass reactor at 623 K during 2h under H_2S/H_2 flow (10% molar in H_2S, 30 mL min^{-1}). For HER experiments and characterization with ex-situ sulfidation, the reactor was then cooled down under Ar and transferred in a dry glovebox under Ar flow to avoid air contact.

2.2. Physico-chemical characterization of the series of catalysts

The X-ray powder diffraction (XRD) patterns were recorded on a XPERT-PRO diffractometer (Cuα radiation λ = 1.5401 Å) in the 2θ range of 5-75° at a scanning rate of 1° min^{-1}, analyzing the samples in their sulfide form. Prior to the analysis, 100 mg of sample was sulfided ex situ (conditions above described) and subsequently placed into an adapted silicon sample holder.
Nitrogen adsorption/desorption isotherms of sulfide catalysts and support were measured at 77 K using Micrometrics Model ASAP 2020 volumetric adsorption analyzer. The catalysts were analyzed in their sulfide form. The catalysts were sulfided ex situ and degassed at 393 K under vacuum for 12 h prior to analysis. Specific surface areas were determined from the BET equation. The total pore volume was calculated from the volume adsorbed at $P/P^0 = 0.95$.

The elemental contents of Co, Mo, Pt and S in sulfide catalysts were determined by ICP-MS method. In a glove box under Ar flow, 50.0 mg of sulfide catalyst were precisely weighed and dissolved in hydrofluoric acid, aqua regia, boric acid, and water with a total volume of 100 ml. Metals and sulfur amounts present in the catalysts were quantified by an inductively coupled plasma mass spectrometry (ICP-MS) using an Agilent quadrupole ICP/MS 7900 equipped with a 1.5 mm Quartz torch and a Helium collision cell.

FTIR was used to explore the effect of CA in the formation of surface functional groups. The carbon supported catalysts were diluted at 5% wt. with KBr FT-IR grade, ≥99%, from Sigma-Aldrich. IR spectra were recorded with a Thermo Nicolet Nexus FT-IR spectrometer equipped with an MCT detector. Prior to the analysis, the sample was evacuated until reaching a residual pressure ~1.10^{-4} Pa. All spectra were normalized to the mass of sample.

2.3. Electron Microscopy Observation by HR STEM-HAADF

The nanostructure and morphology of the slabs were analyzed by high resolution scanning transmission electron microscopy (HR STEM) using a high angle annular dark field (HAADF) detector. The microscopy images were collected using a double corrected JEOL ARM 200F cold FEG microscope operated at 200 kV. The catalysts were observed in their sulfide form. The sulfide catalysts were deposited on a 300-mesh copper grid with holey carbon film. The image treatment was carried out using the commercial software GMS3 from GATAN (DIGITALMICROGRAPH) and free Mesurim software. All of the HR STEM images presented in this work were collected in HAADF mode. The acquisition of one image lasted about 30 s with a resolution of 1024 pixels × 1024 pixels, (30 μs of exposure time for each spot in the scanning mode). Length distribution was obtained by measuring at least 100 slabs per sample.

2.4. Catalytic studies

2.4.1 Thiophene hydrodesulfurization test

The thiophene hydrodesulfurization (HDS) tests were carried out within a differential glass reactor. The procedure followed in this work has been reported in previous publications.[23,25,27] A small amount of catalysts (25 - 50 mg) was loaded in the reactor without diluent. Sulfidation procedure before thiophene HDS test, was performed at 623 K with a heating rate of 3 $K.min^{-1}$ at atmospheric pressure for 2 h under a 30 $mL.min^{-1}$ flow of 10% H_2S/H_2. Later, keeping the 623 K temperature, thiophene HDS test was carried out at the same pressure conditions. Thiophene (Alfa Aesar, 99%, extra pure) was introduced into the reactor by passing 70 $mL.min^{-1}$ of H_2 flow through a saturator kept at 291 K and mixed with a flow of 20 $ml.min^{-1}$ of 10%H_2S/H_2 to keep steady state and avoid the possible reduction of the catalyst. The partial pressures of thiophene, H_2 and H_2S in the mixture were 8 kPa, 90.2 kPa, and 1.8 kPa, respectively. The outflow gas of the HDS reaction was analyzed with a Varian 3900 chromatograph equipped with a Varian Factor 4 (VF-1MS) capillary column (15 m, 0.25 mm,

0.25 µm) and a flame ionization (FID) detector. To maintain a differential reactor, the thiophene conversion was controlled below 10%. The reaction rate (r_s) ($mol.h^{-1}.kg^{-1}$) was calculated using the following formula:

$$r_s = \frac{x \times F}{m_{cat}} \qquad (1)$$

Where x is the thiophene conversion (%), F is the molar flow rate of thiophene ($mol.h^{-1}$) and m_{cat} is the mass of the catalyst after sulfidation, respectively. The mass of the catalyst in reaction was corrected by precisely weighting the catalyst after sulfidation.

2.4.2 HER (Hydrogen Evolution Reaction) Electrochemical Characterizations

Homogenous catalytic inks were prepared by mixing the catalyst powder, a Nafion® suspension (5 wt. % in *n*-propanol), isopropanol, and ultrapure water (Millipore, 18.2 MΩ cm at T = 293 K, total organic compounds < 3 ppb). An aliquot of this ink was then deposited onto the working electrode, a glassy carbon disk of 5 mm diameter. Then, the Nafion® and other solvents were evaporated. The catalyst loading was 300 $\mu g_{powder}\ cm^{-2}$ for the electrochemical characterizations. All electrochemical measurements were carried out using a bi-potentiostat (Autolab PGSTAT302N) operated with NOVA 2.0 software. The totality of the glassware used in this work was cleaned using a H_2SO_4/H_2O_2 (50 % v/v) solution before use. We used a four-electrode electrochemical cell thermostated at T = 298 K. A carbon plate and a freshly prepared home-made reversible hydrogen electrode (RHE) were used as counter-electrode and reference electrode, respectively. The electrochemical experiments were carried out using a rotating disk electrode. For each sample, 10 HER cyclic voltammograms (CVs) were recorded between 0.1 and -0.3 V *vs*. RHE at v = 10 mV. s^{-1} in Ar-saturated 0.5 M H_2SO_4 electrolyte at T = 298 K and at 1600 rpm. The metric used to compare the different electrocatalysts was the value of the overpotential reported at a current density of 10 $mA.cm^{-2}$ (η_{10}). All electrochemical data were iR corrected, where the solution resistances were determined by Electrochemical Impedance Spectroscopy experiments.

3. RESULTS

3.1. Support and MoS_2 phase characterization

The Vulcan XC-72 support was first analyzed to confirm that the carbon structure does not undergo crystalline alterations due to the high temperature (623 K) to which it is subjected during sulfidation (Figure 1A). The broad diffraction peaks located at 2θ values of ~26° and ~43° are attributed to the reflections from the (002) and (101) planes of the hexagonal graphite structure of carbon blacks. No structural change of the support after sulfidation was detected by XRD since both spectra (Figure 1A), before and after sulfidation, appeared practically the same.

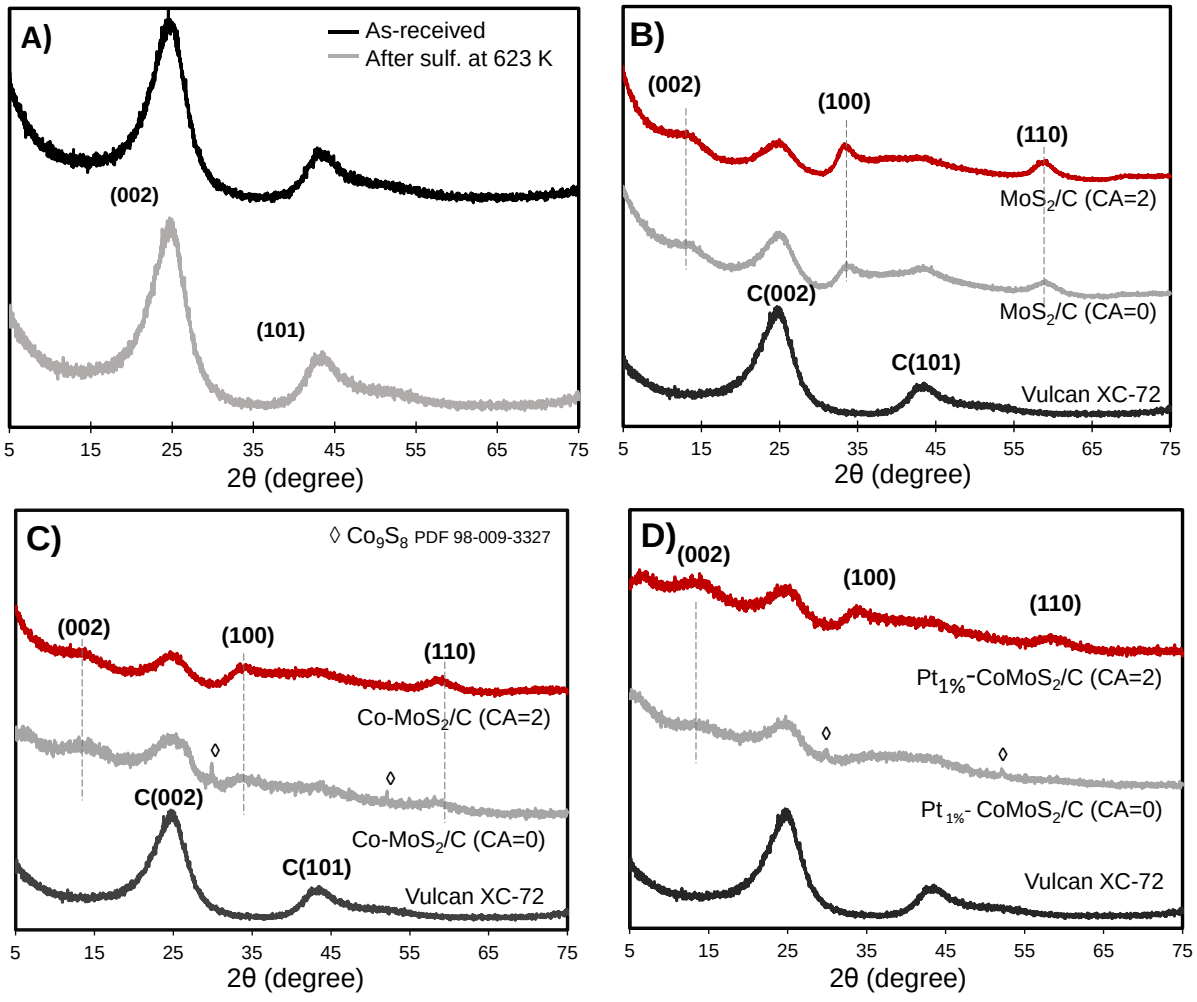

Figure 1. XRD patterns of carbon support (A) and evidence of MoS_2 phase formation on (B) MoS_2/C, (C) Co-MoS_2/C and (D)$Pt_{1\%}$-$CoMoS_2$/C prepared with and without citric acid.

X-ray diffraction (XRD) patterns of the sulfide catalysts with the limit CA concentrations (CA/M=0 and CA/M=2) of each group are shown in (Figure 1B-D). The patterns evidenced them as poorly crystalline materials. However, the existence of a crystalline MoS_2 2H phase is revealed by the (002), (100) and (110) diffraction peaks at 2θ=13.9°, 33.1°, and 58.6°, respectively, with a

typical interlayer spacing of ~6.4 Å (PDF 98-002-1880). Moreover, the broad diffraction peaks ascribed to MoS_2 are indicative of the formation of nanosized particles. In both cases of the Co-MoS_2/C and $Pt_{1\%}$-$CoMoS_2$/C AC=0 catalysts (Figure 1C-D), there are two detected signals at 29.8° and 52.1° corresponding to Co_9S_8 (PDF No. 98-009-3327). CA addition provokes the disappearance of the signal associated to Co_9S_8. It is known that chelating agents such CA, influence the kinetics of chemical processes during the activation step and positively impact the properties of the resulting sulfide. In this case, CA favors the dispersion and promotion (integration of Co in the edges) of the sulfide slabs.[21] This is attributed to enhanced reducibility of molybdenum as well as to lowered metal-support interactions.[28] No Pt associated signals could be detected by XRD. The existence of Pt in the catalysts is later confirmed by STEM HAADF.

The nitrogen adsorption−desorption isotherms of the Vulcan XC-72 support and of the sulfided catalysts (CA/M=0 and CA/M=2) correspond to a type IV isotherm according to IUPAC classification with a H1 hysteresis loop, characteristic for mesoporous materials (SI-1).[29] At partial pressures close to unity, no saturation is observed, which provides evidence for the presence of macropores and which is interpreted as an indication of the presence of large aggregates of particles. Table 1 shows the corresponding surface area values obtained for the catalysts. Overall, a decrease of the total surface is detected, which suggests a partial blockage of the porosity. This blockage is not linked with the presence or not of CA; nor with the temperature of sulfidation since carbon Vulcan demonstrated to keep the surface area after sulfidation at 350 °C. The formation of MoS_2 slabs should be responsible for some aggregation of the C particles through weak interaction.

Elemental composition was determined by ICP-MS after the sulfidation stage of the catalysts in order to verify the sulfidation degree of the carbon supported Co-MoS_2 and $Pt_{1\%}$-$CoMoS_2$ catalysts (Table 2). All the catalysts presented enough sulfur to form MoS_2 ; i.e., the molar concentration of sulfur present in the sample is about twice that of Mo. It is also observable that the S/M ratio increased progressively with the citric acid content. Thus, this is an indication that adding citric acid into the preparation favors the sulfidation of Mo.

Table 1: BET surface area of the support and sulfide catalysts

Samples	S_{BET} ($m^2 g^{-1}$)

Vulcan XC 72	229
« sulfided » Vulcan XC72	241
MoS_2/C (CA=0)	116
MoS_2/C (CA=2)	140
Co-MoS_2/C (CA=0)	100
CoMo S_2/C (CA=2)	181
$Pt_{1\%}$- $CoMoS_2$/C (CA=0)	90
$Pt_{1\%}$-$CoMoS_2$/C (CA=2)	65

Table 2: ICP analysis of the sulfided samples

Sulfide Catalyst	Mo wt. %	Co wt. %	Pt wt. %	Co/(Co+Mo)[a]	S/Mo[a]
Mo/C (CA=0)	16	-	-	-	1,7
Mo/C (CA=1)	14	-	-	-	2,0
Mo/C (CA=2)	14	-	-	-	2,4
Co-MoS_2/C (CA=0)	15	4	-	0,3	1,7
Co-MoS_2/C (CA=1)	14	4	-	0,3	1,9
Co-MoS_2/C (CA=2)	14	4	-	0,3	2,2
$Pt_{1\%}$- $CoMoS_2$/C (CA=0)	15	4	1	0,3	1,9
$Pt_{1\%}$- $CoMoS_2$/C (CA=1)	15	4	1	0,3	2,1
$Pt_{1\%}$- $CoMoS_2$/C (CA=2)	14	4	1	0,3	2,3

[a]Atomic ratio

The MoS_2/C sample prepared with and without CA was analyzed by IR spectroscopy to explore the effect of the chelating agent on the support surface (Figure 2). In both catalysts a strong band at 1590 cm^{-1} is observed and assigned to the ν (C=C) vibrations of the sp2 rings, characteristic of the carbon support backbone. It is also observed that for both catalysts, functional groups such as CH, OH and -COOH groups are present. However, these groups are less abundant in the support without CA.

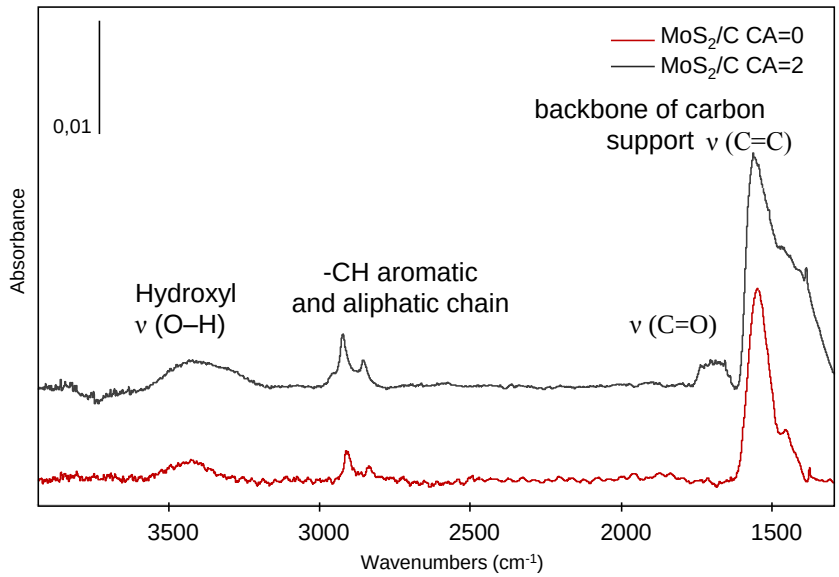

Figure 2. IR spectra of MoS_2/C catalyst prepared with and without citric acid (transmission IR with dilution in KBr).

In order to analyze the morphology of the sulfide catalyst particles, STEM-HAADF observation was performed on the catalysts prepared without CA Figure (A, C, E) and with CA/M ratio equal 2 (Figure (B, D, F). Figure G and H show the corresponding particle size distributions. The addition of citric acid to the (Co) (Pt) Mo catalysts tends to decrease the size of the particles. Comparing MoS_2/C (CA = 0)/C and MoS_2/C (CA = 2)/C catalysts, the addition of citric acid leads to a decrease of the average slab length from 2.10 ± 0.12 nm to 1.40 ± 0.20 nm. As reported previously, the three catalysts with CA/M=2 have similar average slab length around 1.40 nm [19].

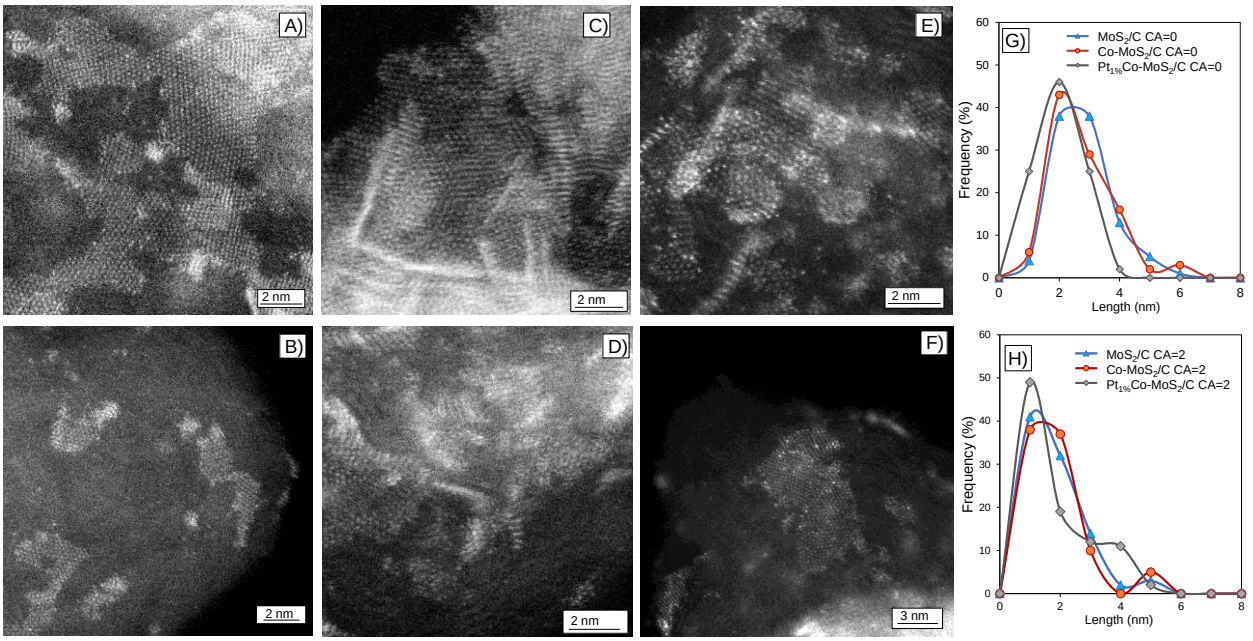

Figure 3. STEM-HAADF images of some particles from (A) MoS_2/C (CA=0), (B) MoS_2/C (CA=2), (C) Co-MoS_2/C (CA=0), (D) Co-MoS_2/C (CA=2), (E) $Pt_{1\%}$-$CoMoS_2$ (CA=0) and (F) $Pt_{1\%}$-$CoMoS_2$ (CA=2). Length frequency histograms (G) catalysts without CA and (H) with CA = 2.

During this acquisition and despite exposure to the electron beam, the shapes of the particles remained unchanged, this agrees with the conductive character of carbon, meaning that the slabs were quite stable under the electron beam. For the $Pt_{1\%}$-$CoMoS_2$ catalysts, the platinum atoms seem to be only integrated within the MoS_2 slabs, no Pt clusters are distinguished. Note that the Pt atoms appear with a much brighter contrast due to the higher Z value (78) compared to those of Mo (42) and Co (27). More particularly, it is observed that the Pt atom integration occurs mainly at the edges of the slabs, thus functioning as a promoter atom. However, some atoms can also be found integrated inside the slab. An observed peculiarity is that as the exposure time to the electron beam progresses, the Pt atoms located at the edge are mobile under the beam (brightest dots indicated by arrows in Figure 4), in some cases agglomerating and in others returning to their initial position. It is observed that those Pt atoms located in the inner part of the slab are stable and do not change their position. This phenomenon was neither observed in the case of peripheric Mo or Co atoms.

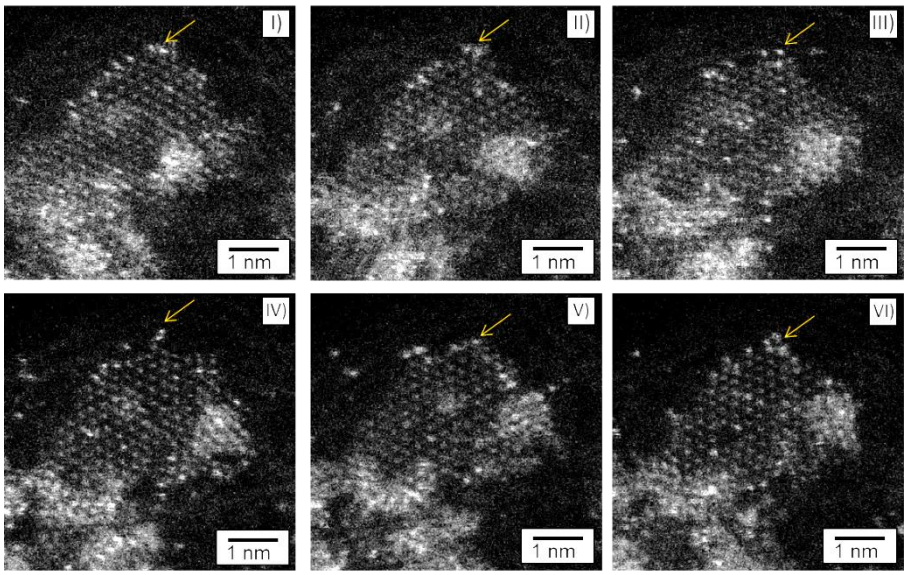

Figure 4. STEM-HAADF images of similar zone of the $Pt_{1\%}$-$CoMoS_2$/C (AC=2) showing atomic Pt mobility during exposure to electron beam

3.2. ***Hydrogen Evolution Reaction (HER) activity***

The HER electrocatalytic activity of the three-catalyst series (MoS_2/C, Co-MoS_2/C and $Pt_{1\%}$-$CoMoS_2$/C) prepared with and without citric acid was measured by cyclic voltammetry in liquid

acidic electrolyte. Figure 5 shows the HER electrochemical results for the three catalysts and for different values of CA/M ratio (CA/M= 0, 1 2 or 3 and M=Mo+Co+ Pt). The comparison of the overpotential (η_{10}) measured at 10 mA.cm^{-2} which is the descriptor currently used shows the beneficial role of citric acid on the HER activity (Figure 5C). Catalysts prepared with citric acid present a lower overpotentials (η_{10}) than the ones with no addition of the CA. These results agree with the higher density of exposed edge active sites on slabs with smaller length size. For the Co-MoS_2/C and $Pt_{1\%}$-$CoMoS_2$/C), an optimal value of CA/M is reported around CA = 2. Beyond this ratio, HER activity starts to decrease. Among all, the $Pt_{1\%}$-$CoMoS_2$/C (CA= 2) exhibits the lowest value of 0.120 V *vs.* RHE presenting the superior HER activity. The Tafel slope is also a good indicator of HER kinetic aspects. Interestingly, all the Tafel slopes are in the same order of magnitude, between 60 and 75 mV decade^{-1} suggesting that mechanistic steps should be similar. In addition, the higher value of the Tafel slopes of this class of sulfide catalyst with respect to Pt/C one confirms the slower HER kinetics of this class of sulfide catalysts compared to Pt/C catalyst [30,31]. For Pt/C catalyst, the Tafel step that is the recombination of two H_{ads} leading molecular H_2 is considered as the rate determining step. For our sulfide catalysts, the rate determining step should be a combination of Volmer-Heyrovsky step (adsorption of the first proton followed by its reaction with a water molecule to product molecular H_2) as indicated by the higher value of the Tafel slope.

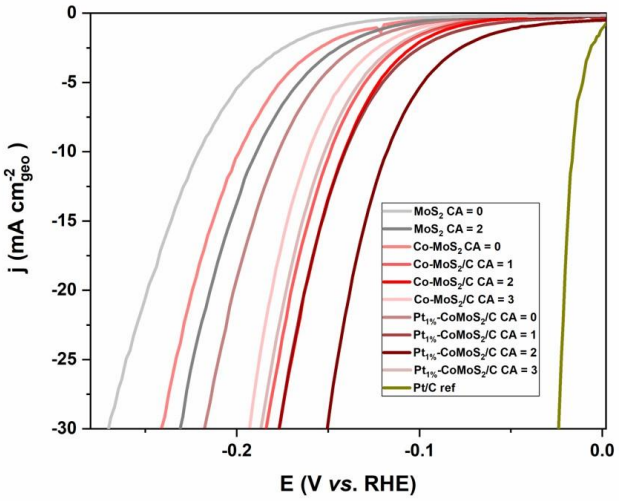
0
-5
-10
-15
-20
-25
-30
-0.2
-0.1
0.0
j (mA cm-2geo)
E (V vs. RHE)
MoS2 CA = 0
MoS2 CA = 2
Co-MoS2 CA = 0
Co-MoS2/C CA = 1
Co-MoS2/C CA = 2
Co-MoS2/C CA = 3
Pt1%-CoMoS2/C CA = 0
Pt1%-CoMoS2/C CA = 1
Pt1%-CoMoS2/C CA = 2
Pt1%-CoMoS2/C CA = 3
Pt/C ref

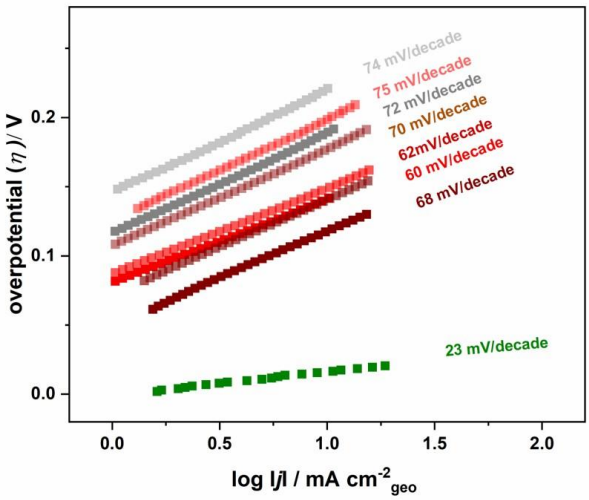
overpotential (η)/ V
0.2
0.1
0.0
0.0
0.5
1.0
1.5
2.0
log |j| / mA cm-2geo
74 mV/decade
75 mV/decade
72 mV/decade
70 mV/decade
62mV/decade
60 mV/decade
68 mV/decade
23 mV/decade

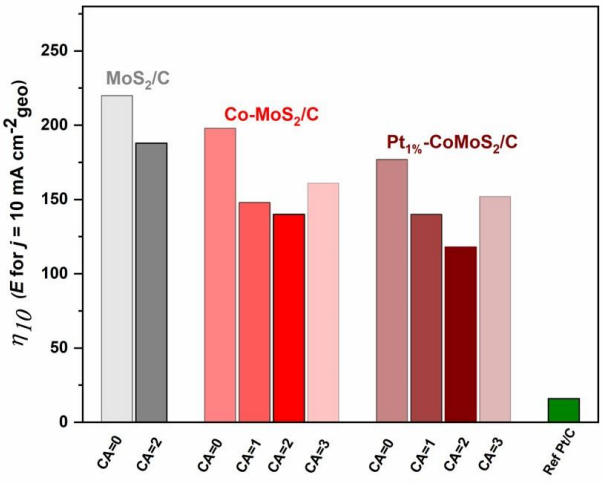
η10 (E for j = 10 mA cm-2geo)
250
200
150
100
50
0
MoS2/C
Co-MoS2/C
Pt1%-CoMoS2/C
CA=0
CA=2
CA=0
CA=1
CA=2
CA=3
CA=0
CA=1
CA=2
CA=3
Ref Pt/C

Figure 5: ***HER activity measurements.*** *A) polarization curves, B) Tafel plots and C) overpotential measured at 10 mA cm^{-2} (η_{10}) for MoS_2/C, Co-MoS_2/C, $Pt_{1\%}$-$CoMoS_2$/C catalysts synthesized with different ratio of CA/M. The HER polarization curves were performed in Ar-saturated 0.5 M H_2SO_4, ω = 1600 rpm, $v = 10\ mV\ s^{-1}$, T = 298 K. The catalyst's loading was 300 $\mu g_{powder}\ cm^{-2}$*

3.3. Hydrodesulfurization (HDS) activity

In thiophene HDS, as expected, the lowest catalytic activity was observed for the non-promoted catalysts series, nevertheless it was observed that the addition of citric acid increased the activity of MoS_2/C, the increase being stronger with higher CA/M ratio up to the tested value of 2 (Figure 6). Similar behavior had already been reported for MoS_2/Al_2O_3 prepared with increasing CA/M ratio.[32] The promotion by Co does increase significantly the activity and for this series, the effect of citric acid is even more pronounced than for the Mo series. Note however that there is a CA/M limit since the addition of CA with a ratio of CA/M =3 leads to lower activity than with the ratio CA/M=2. Such a limit has been previously reported for chelating agent addition effect on HDS activity and explained by over stoichiometry as compared to the complex stoichiometry [33,34]. For the trimetallic series, the addition of Pt further increases the activity of the catalysts while the effect of CA is similar to the one for the CoMo series.

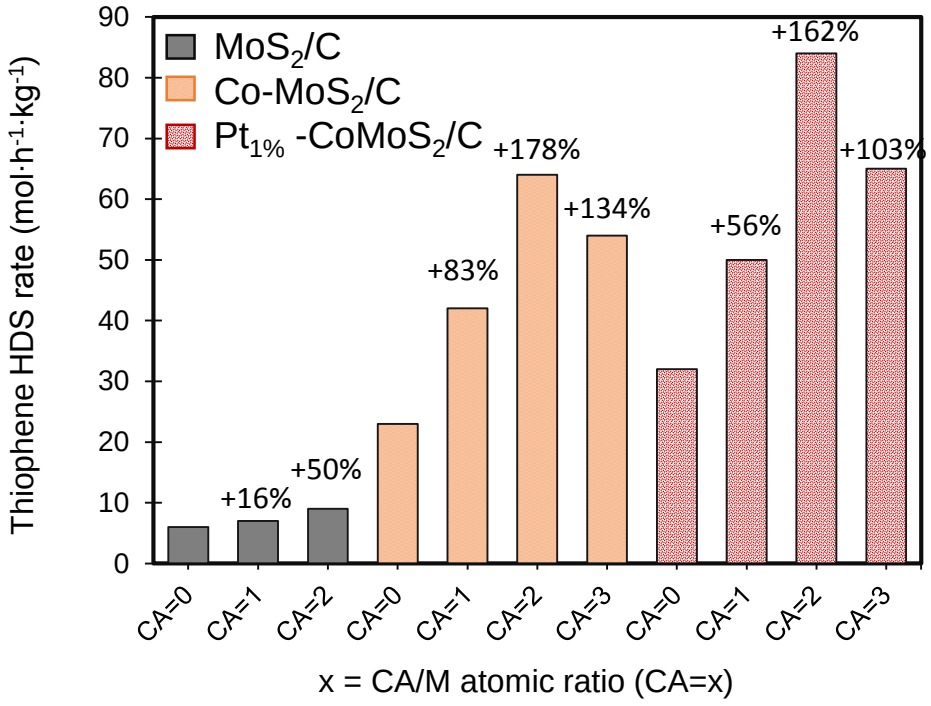

Figure 6: Thiophene HDS rate on (Co)(Pt)MoS_2/C: effect of the CA/M ratio. The percentage gives the increase in activity with CA compare to the corresponding reference catalyst with no CA (CA=0)

4. DISCUSSION: COMPARISON BETWEEN HDS AND HER ACTIVITY

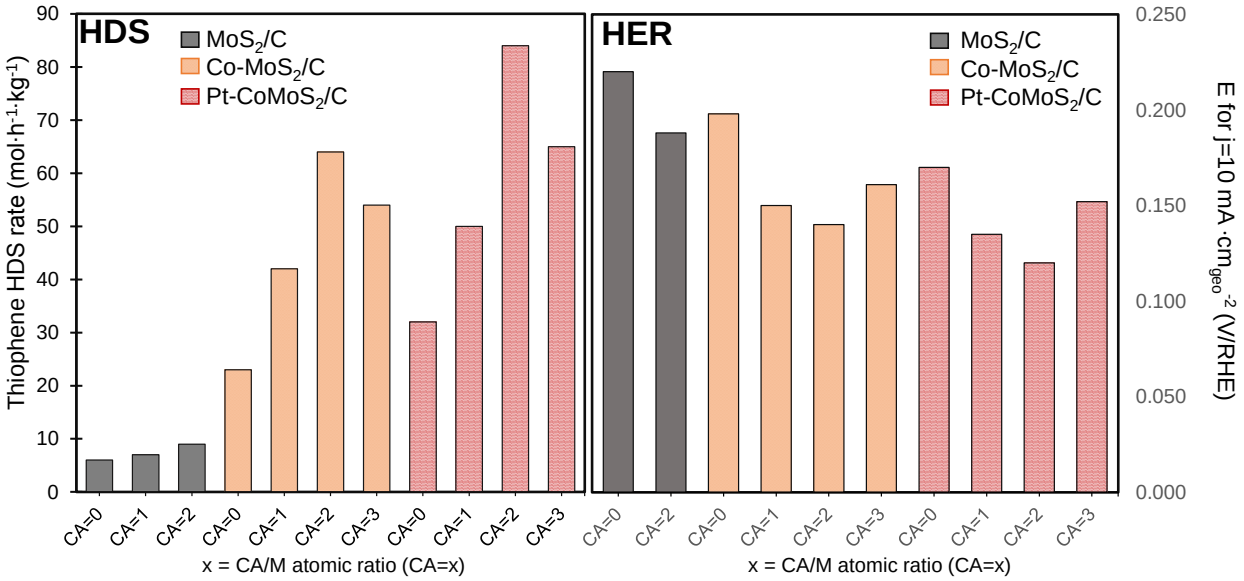

Figure 7. Parallel between HDS and HER activity

For both reactions, there is a similar activity trend on the three-catalyst series. In general, the best catalyst in HDS is also the best catalyst in HER, and in turn, the least performing in HDS is also the least performing in HER. Whatever the CA/M ratio, addition of Co increases the activity for both reactions and addition of platinum strengthen the effect. With the three types of catalysts, it is observed that the use of citric acid during the preparation increases the catalytic activity in both types of reaction and that optimum performance is achieved with the addition of citric acid in a CA/M =2 proportion. This positive effect of CA could be partly linked to a decrease in slab length as revealed by STEM-HAADF for Mo and $Pt_{1\%}$CoMo catalysts and to the higher sulfidation degree as revealed by ICP-MS. Finally, an excess of citric acid, that is, CA/M=3, causes a decrease in the catalytic activity for both HDS and HER. Note however, that the activity change from one composition to another in HDS cannot be directly converted to the activity change in HER since the activity parameters are not the same at all (activity rate in HDS versus overpotential at 10 $mA.cm^{-2}$ for HER). In particular, the extent of activity modification with catalyst composition is not the same for both reactions. However, this similar variation of activity with the catalyst composition and preparation mode goes well with the initial idea that similar

edge sites are involved in both reactions. Knowledge acquired on HDS catalysts optimization can be extended to the design of HER electrocatalysts. This is in accordance with the activity descriptor for HDS being the M-S bond strength [35] and the one for HER being the Gibbs free energy of H adsorption, since these descriptors can be linked to each other's: in both reactions adsorption of H should occur on the M-S bond. Interestingly, the low amount of Pt added is revealed as single Pt atoms dispersed on the edge of the MoS_2 slab (see Figures 3E, 3F and 4). Although some Pt atoms mobility could be observed on the edge of the slabs, previous in-situ ICP-MS analysis of the electrolyte during HER test reveals that this mobility is not associated with leaching of the Pt atoms. Thus, MoS_2 appears as a stabilizing support for single Pt atoms.

5. CONCLUSIONS

Molybdenum sulfide catalysts supported on carbon have been prepared with different citric acid on metal ratio and with promotion by Co and/or Pt atoms. Activity in HER Reaction (HER) was found to benefit from the addition of citric acid with an optimal proportion of chelating agent on metal of two. Promotions by Co and Co+Pt were also beneficial to the HER activity but without reaching the one of the reference Pt/C catalyst. Similar effects of promotion and chelating agent addition are obtained on HDS thiophene activity. This parallel in activity modification is ascribed to the involvement of the same edge sites as active sites and to the relevance of H adsorption mechanism step in both reactions. Thus, the design of MoS_2 based HER catalyst could benefit from its optimization for HDS reactions.

ACKNOWLEDGEMENTS

The authors acknowledge the financial support of ANR CARNOT Energie et Systemes` de Propulsion (ESP) and ANR CARNOT Energies du Futur (EF) through the HERMOS project.

DECLARATION OF COMPETING INTEREST

The authors declare that they have no known competing financial interests or personal relationships that could have appeared to influence the work reported in this paper.

REFERENCES

[1] I. Dresselhaus, M., Thomas, Alternative energy technologies., Nature. 414 (2001) 332–337. https://doi.org/https://doi.org/10.1038/35104599.

[2] G. Fu, J.M. Lee, Ternary metal sulfides for electrocatalytic energy conversion, J. Mater. Chem. A. 7 (2019) 9386–9405. https://doi.org/10.1039/c9ta01438a.

[3] S.E. Hosseini, Hydrogen from solar energy , a clean energy carrier from a sustainable source of energy, (2020) 4110–4131. https://doi.org/10.1002/er.4930.

[4] T.F. Jaramillo, K.P. Jørgensen, J. Bonde, J.H. Nielsen, S. Horch, I. Chorkendorff, Identification of active edge sites for electrochemical H2 evolution from MoS2 nanocatalysts, Science (80-.). 317 (2007) 100–102. https://doi.org/10.1126/science.1141483.

[5] Y. Cao, Roadmap and Direction toward High-Performance MoS2Hydrogen Evolution Catalysts, ACS Nano. 15 (2021) 11014–11039. https://doi.org/10.1021/acsnano.1c01879.

[6] J.N. Hansen, H. Prats, K.K. Toudahl, N. Mørch Secher, K. Chan, J. Kibsgaard, I. Chorkendorff, Is There Anything Better than Pt for HER?, ACS Energy Lett. 6 (2021) 1175–1180. https://doi.org/10.1021/acsenergylett.1c00246.

[7] P.C.K. Vesborg, B. Seger, I. Chorkendorff, Recent development in hydrogen evolution reaction catalysts and their practical implementation, J. Phys. Chem. Lett. 6 (2015) 951–957. https://doi.org/10.1021/acs.jpclett.5b00306.

[8] J.D. Benck, T.R. Hellstern, J. Kibsgaard, P. Chakthranont, T.F. Jaramillo, Catalyzing the hydrogen evolution reaction (HER) with molybdenum sulfide nanomaterials, ACS Catal. 4 (2014) 3957–3971. https://doi.org/10.1021/cs500923c.

[9] Z. Wang, B. Mi, Environmental Applications of 2D Molybdenum Disulfide (MoS2) Nanosheets, Environ. Sci. Technol. 51 (2017) 8229–8244. https://doi.org/10.1021/acs.est.7b01466.

[10] Z. Lei, J. Zhan, L. Tang, Y. Zhang, Y. Wang, Recent Development of Metallic (1T) Phase

of Molybdenum Disulfide for Energy Conversion and Storage, Adv. Energy Mater. 8 (2018) 1–29. https://doi.org/10.1002/aenm.201703482.

[11] Q. Lu, Y. Yu, Q. Ma, B. Chen, H. Zhang, 2D Transition-Metal-Dichalcogenide-Nanosheet-Based Composites for Photocatalytic and Electrocatalytic Hydrogen Evolution Reactions, Adv. Mater. 28 (2016) 1917–1933. https://doi.org/10.1002/adma.201503270.

[12] J.V. Lauritsen, M. Nyberg, J.K. Nørskov, B.S. Clausen, H. Topsøe, E. Lægsgaard, F. Besenbacher, Hydrodesulfurization reaction pathways on MoS2 nanoclusters revealed by scanning tunneling microscopy, J. Catal. 224 (2004) 94–106. https://doi.org/10.1016/J.JCAT.2004.02.009.

[13] C. Wivel, R. Candia, B.S. Clausen, S. Mørup, H. Topsøe, On the catalytic significance of a CoMoS phase in CoMo Al2O3 hydrodesulfurization catalysts: Combined in situ Mössbauer emission spectroscopy and activity studies, J. Catal. 68 (1981) 453–463. https://doi.org/10.1016/0021-9517(81)90115-9.

[14] H. Topsøe, B.S.. Clausen, F.E.. Massoth, Catalysis Science and Technology, Springer, Berlin, 1996. https://doi.org/10.1007/978-3-642-61040-0_1.

[15] M. Vrinat, M. Breysse, C. Geantet, J. Ramirez, F. Massoth, Effect of MoS2 morphology on the HDS activity of hydrotreating catalysts, Catal. Letters. 26 (1994) 25–35.

[16] B. Hinnemann, P.G. Moses, J. Bonde, K.P. Jørgensen, J.H. Nielsen, S. Horch, I. Chorkendorff, J.K. Nørskov, Biomimetic hydrogen evolution: MoS2 nanoparticles as catalyst for hydrogen evolution, J. Am. Chem. Soc. 127 (2005) 5308–5309. https://doi.org/10.1021/ja0504690.

[17] Z. Luo, Y. Ouyang, H. Zhang, M. Xiao, J. Ge, Z. Jiang, J. Wang, D. Tang, X. Cao, C. Liu, W. Xing, Chemically activating MoS2 via spontaneous atomic palladium interfacial doping towards efficient hydrogen evolution, Nat. Commun. 9 (2018) 1–8. https://doi.org/10.1038/s41467-018-04501-4.

[18] W. Wang, Y. Song, C. Ke, Y. Li, Y. Liu, C. Ma, Z. Wu, J. Qi, K. Bao, L. Wang, J. Wu, S. Jiang, J. Zhao, C.S. Lee, Y. Chen, G. Luo, Q. He, R. Ye, Filling the Gap between Heteroatom Doping and Edge Enrichment of 2D Electrocatalysts for Enhanced Hydrogen

Evolution, ACS Nano. 17 (2023) 1287–1297. https://doi.org/10.1021/acsnano.2c09423.

[19] L.A. Zavala, K. Kumar, V. Martin, F. Maillard, F. Maugé, X. Portier, L. Oliviero, L. Dubau, Direct Evidence of the Role of Co or Pt, Co Single-Atom Promoters on the Performance of MoS2 Nanoclusters for the Hydrogen Evolution Reaction, ACS Catal. 13 (2023) 1221–1229. https://doi.org/10.1021/acscatal.2c05432.

[20] J. Chen, F. Mauge, J. El Fallah, L. Oliviero, IR spectroscopy evidence of MoS2 morphology change by citric acid addition on MoS2/Al2O3 catalysts - A step forward to differentiate the reactivity of M-edge and S-edge, J. Catal. 320 (2014) 170–179. https://doi.org/10.1016/j.jcat.2014.10.005.

[21] L. Oliviero, F. Maugé, P. Afanasiev, C. Pedraza-Parra, C. Geantet, Organic additives for hydrotreating catalysts: A review of main families and action mechanisms, Catal. Today. 377 (2021) 3–16. https://doi.org/10.1016/j.cattod.2020.09.008.

[22] J. Chen, J. Mi, K. Li, X. Wang, E. Dominguez Garcia, Y. Cao, L. Jiang, L. Oliviero, F. Oise, Role of Citric Acid in Preparing Highly Active CoMo/Al 2 O 3 Catalyst: From Aqueous Impregnation Solution to Active Site Formation, Ind. Eng. Chem. Res. 56 (2017) 14172–14181. https://doi.org/10.1021/acs.iecr.7b02877.

[23] L.A. Zavala-Sanchez, X. Portier, F. Maugé, L. Oliviero, Promoter Location on NiW/Al2O3Sulfide Catalysts: Parallel Study by IR/CO Spectroscopy and High-Resolution STEM-HAADF Microscopy, ACS Catal. 10 (2020) 6568–6578. https://doi.org/10.1021/acscatal.0c01092.

[24] L. Zavala-Sanchez, X. Portier, F. Maugé, L. Oliviero, Formation and stability of CoMoS nanoclusters by the addition of citric acid: A study by high resolution STEM-HAADF microscopy, Catal. Today. 377 (2021) 127–134. https://doi.org/10.1016/j.cattod.2020.10.039.

[25] L.A. Zavala-sanchez, F. Maugé, X. Portier, L. Oliviero, Infrared Spectroscopic Evidence of WS 2 Morphology Change With Citric Acid Addition and Sul fi dation Temperature, 3 (2022) 1–10. https://doi.org/10.3389/fceng.2021.792368.

[26] J. Chen, J. Mi, K. Li, X. Wang, E.D. Garcia, Y. Cao, L. Jiang, L. Oliviero, F. Mauge, Role

of Citric Acid in Preparing Highly Active CoMo/Al2O3 Catalyst: From Aqueous Impregnation Solution to Active Site Formation, Ind. Eng. Chem. Res. 56 (2017) 14172–14181. https://doi.org/10.1021/acs.iecr.7b02877.

[27] L. Zavala-Sanchez, X. Portier, F. Maugé, L. Oliviero, High-resolution STEM-HAADF microscopy on a γ-Al2O3 supported MoS2 catalyst - Proof of the changes in dispersion and morphology of the slabs with the addition of citric acid, Nanotechnology. 31 (2020) 35706. https://doi.org/10.1088/1361-6528/ab483c.

[28] L. Van Haandel, G.M. Bremmer, E.J.M. Hensen, T. Weber, The effect of organic additives and phosphoric acid on sulfidation and activity of (Co)Mo/Al2O3 hydrodesulfurization catalysts, J. Catal. 351 (2017) 95–106. https://doi.org/10.1016/j.jcat.2017.04.012.

[29] R. Bardestani, G.S. Patience, S. Kaliaguine, Experimental methods in chemical engineering: specific surface area and pore size distribution measurements—BET, BJH, and DFT, Can. J. Chem. Eng. 97 (2019) 2781–2791. https://doi.org/10.1002/cjce.23632.

[30] H. Li, C. Tsai, A.L. Koh, L. Cai, A.W. Contryman, A.H. Fragapane, J. Zhao, H.S. Han, H.C. Manoharan, F. Abild-Pedersen, J.K. Nørskov, X. Zheng, Activating and optimizing MoS2 basal planes for hydrogen evolution through the formation of strained sulphur vacancies, Nat. Mater. 15 (2016) 364. https://doi.org/10.1038/nmat4564.

[31] B.E. Conway, B. V. Tilak, Interfacial processes involving electrocatalytic evolution and oxidation of H2, and the role of chemisorbed H, Electrochim. Acta. 47 (2002) 3571–3594. https://doi.org/10.1016/S0013-4686(02)00329-8.

[32] J. Chen, F. Maugé, J. El Fallah, L. Oliviero, IR spectroscopy evidence of MoS2 morphology change by citric acid addition on MoS2/Al2O3 catalysts – A step forward to differentiate the reactivity of M-edge and S-edge, J. Catal. 320 (2014) 170–179. https://doi.org/10.1016/j.jcat.2014.10.005.

[33] M.A. Lélias, P.J. Kooyman, L. Mariey, L. Oliviero, A. Travert, J. van Gestel, J.A.R. van Veen, F. Maugé, Effect of NTA addition on the structure and activity of the active phase of cobalt-molybdenum sulfide hydrotreating catalysts, J. Catal. 267 (2009) 14–23. https://doi.org/10.1016/j.jcat.2009.07.006.

[34] L. Oliviero, F. Maugé, P. Afanasiev, C. Pedraza-Parra, C. Geantet, Organic additives for hydrotreating catalysts: A review of main families and action mechanisms, Catal. Today. 377 (2021) 3–16. https://doi.org/10.1016/j.cattod.2020.09.008.

[35] H. Toulhoat, P. Raybaud, Catalysis by Transition Metal Sulfides: from molecular theory to industrial application, Edition technip, Paris, 2013.

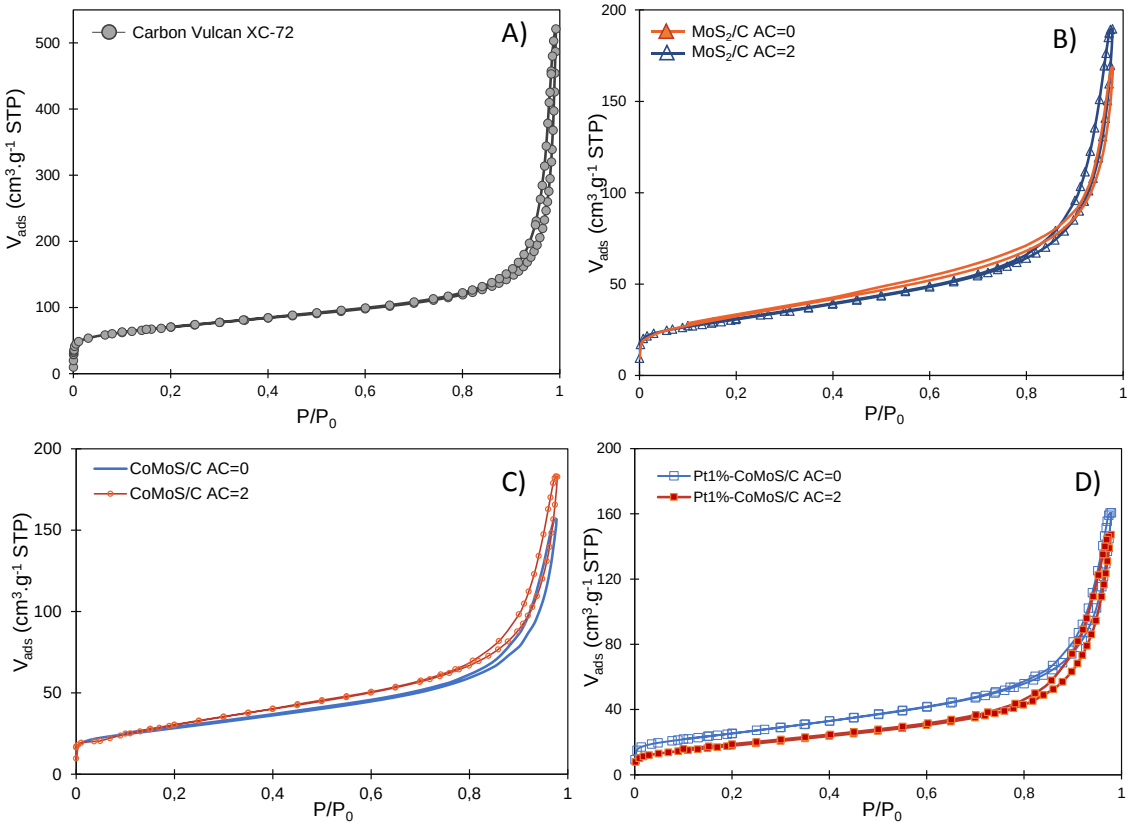

SI.1. N2 adsorption isotherms for Vulcan XC-72 (A) and for the carbon supported catalysts.